ACS APPLIED MATERIALS & INTERFACES

www.acsami.org

Research Article

Formation of Head/Tail-to-Body Charged Domain Walls by Mechanical Stress

Qianwei Huang, Jiyuan Yang, Zibin Chen,* Yujie Chen, Matthew J. Cabral, Haosu Luo, Fei Li, Shujun Zhang, Yulan Li, Zonghan Xie, Houbing Huang, Yiu-Wing Mai, Simon P. Ringer, Shi Liu,* and Xiaozhou Liao*

Cite This: *ACS Appl. Mater. Interfaces* 2023, 15, 2313–2318

Read Online

ACCESS | Metrics & More | Article Recommendations | Supporting Information

Downloaded via WESTLAKE UNIV on January 12, 2023 at 19:02:01 (UTC).
See https://pubs.acs.org/sharingguidelines for options on how to legitimately share published articles.

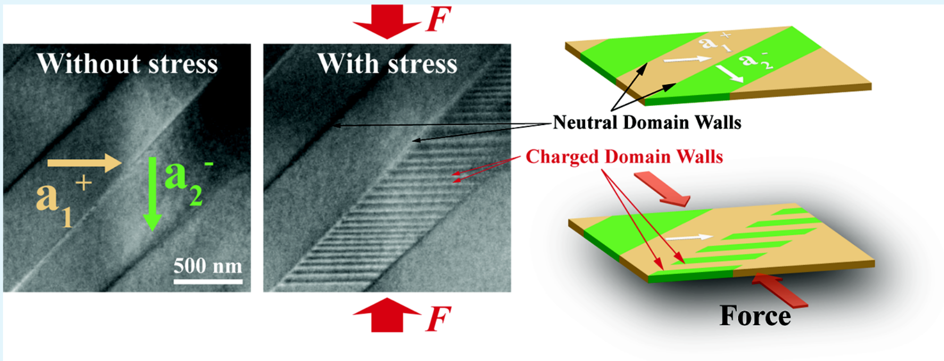

ABSTRACT: Domain walls (DWs) in ferroelectric materials are interfaces that separate domains with different polarizations. Charged domain walls (CDWs) and neutral domain walls are commonly classified depending on the charge state at the DWs. CDWs are particularly attractive as they are configurable elements, which can enhance field susceptibility and enable functionalities such as conductance control. However, it is difficult to achieve CDWs in practice. Here, we demonstrate that applying mechanical stress is a robust and reproducible approach to generate CDWs. By mechanical compression, CDWs with a head/tail-to-body configuration were introduced in ultrathin $BaTiO_3$, which was revealed by in-situ transmission electron microscopy. Finite element analysis shows strong strain fluctuation in ultrathin $BaTiO_3$ under compressive mechanical stress. Molecular dynamics simulations suggest that the strain fluctuation is a critical factor in forming CDWs. This study provides insight into ferroelectric DWs and opens a pathway to creating CDWs in ferroelectric materials.

KEYWORDS: *ferroelectric, charged domain walls, strain gradient, transmission electron microscopy, domain switching*

INTRODUCTION

Ferroelectrics are promising materials for applications in electronic devices because of their tunable polarization under various external stimuli.[1−4] Polarization in ferroelectric materials may vary from one area to another and an area with the same polarization is called a domain. The interfaces/boundaries that separate neighboring domains are called domain walls (DWs).[5] Depending on the charge state at interfaces, DWs can be classified into two types: neutral DWs (NDWs) with no aggregation of net bound charges[6] and charged DWs (CDWs).[7] The positive CDWs are usually of the head-to-head type, as the polarization directions of the surrounding domains point to the DWs, while the negative CDWs are often of the tail-to-tail type, where the polarization directions of the neighboring domains point away from the DWs.[8]

CDWs possess many unique properties that would be utilized in the design of novel electronic devices.[9−12] Bound charges at CDWs can generate considerable depolarization fields that facilitate polarization rotation, resulting in superior electromechanical properties in ferroelectrics.[9] It has been reported that the conductivity of ferroelectric thin films can be drastically enhanced when the length of CDWs exceeds a critical value, making the materials suitable for logical and memory devices owing to a high on/off ratio enabled by the CDW switching.[13] Compared to conventional memories, the memories based on ferroelectric CDWs possess supreme advantages, including their intrinsic nondestructive and nonvolatile functionalities.[14,15] Discoveries into the peculiarities of CDWs have catalyzed the development of CDW-based nanoelectronic devices, including

Received: August 14, 2022
Accepted: November 24, 2022
Published: December 19, 2022

© 2022 American Chemical Society

field-effect transistors,[16] nanocircuits,[17] and artificial neural networks.[18]

The formation of DWs in ferroelectrics is the result of the minimization of system free energy.[19] NDWs are commonly observed in as-fabricated ferroelectrics as such configurations are energetically preferable.[20] On the contrary, natural CDWs rarely form spontaneously without imposing mechanical constraints or appropriate electric boundary conditions.[13,21] A number of strategies, including biasing and/or heating, has been proposed to create CDWs in ferroelectric materials.[8,22,23] Among these, frustrated poling is the most common approach.[22] For example, repeated electric fields are applied along the ⟨110⟩ direction of tetragonal ferroelectrics, and polarizations could occur aligning along either the [100] or the [010] direction, resulting in the formation of either 90° NDWs or 90° CDWs. In this strategy, the formation of CDWs is often uncontrollable and the application of cyclic electric fields would also weaken the ferroelectric properties due to ferroelectric fatigue.[24,25] Therefore, it is of significance to comprehend the underlying mechanisms governing the formation of CDWs and to explore a reliable method of creating a high density of stable CDWs.

In this article, we report the introduction of CDWs in thin $BaTiO_3$ (BTO) micropillars through a strain gradient. The resultant CDWs are a new type of 90° CDW with a unique head/tail-to-body polarization configuration. When an ultrathin (~70 nm) BTO micropillar was subjected to uniaxial compression, emerging nanodomains with newly formed 90° CDWs were recorded in real time by in-situ transmission electron microscopy (TEM).[26,27] This new type of 90° CDW is neither head-to-head nor tail-to-tail, which is dissimilar from previously reported 90° CDWs in tetragonal ferroelectrics.[22,28,29] Finite element analysis (FEA) and molecular dynamics (MD) simulations confirm that strain gradient plays a critical role in forming dense CDWs in ultrathin lamellae. This study transcends the common understanding of DWs and opens a new pathway to creating stable periodic CDWs for domain wall engineering in ferroelectrics.

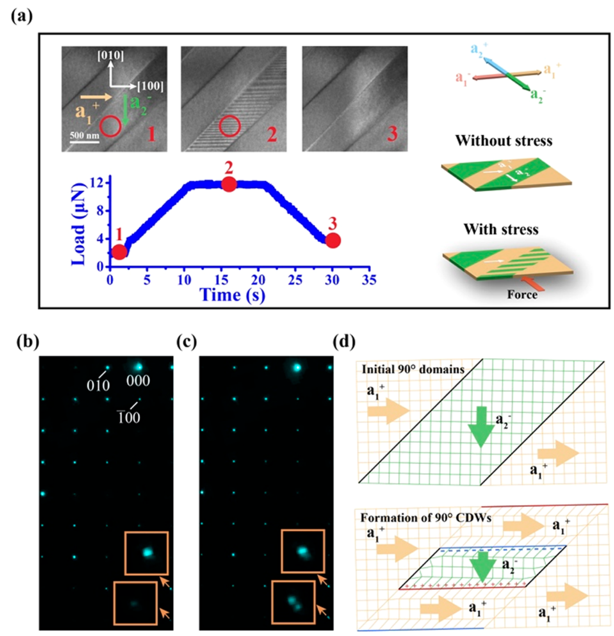

Figure 1. In-situ domain switching behavior under a mechanical loading in an ultrathin BTO micropillar. (a) Load versus time curve showing the real-time application of compressive load to the thin BTO micropillar. The numbers 1, 2, and 3 correspond to the TEM images (extracted from Movie S1) labeled 1, 2, and 3, respectively. Schematic diagrams of the domain configurations without and with the applied stress are presented at the right side. The yellow and green arrows in the TEM images and the white arrows in the schematics denote the polarization directions. The color codes in the top right corner denote the polarizations of a_1 (a_1^+/a_1^-) and a_2 (a_2^+/a_2^-) domains, which are along ± [100] and ± [010] axes, respectively. (b, c) Electron diffraction patterns obtained from the area marked with a red circle in the TEM image in panel a without and with compressive loading, respectively. (d) Schematics illustrating the formation of the head/tail-to-body 90° CDWs under the applied stress. Positive (red) and negative (blue) CDWs are presented alternatively.

■ RESULTS AND DISCUSSION

BTO is a traditional ferroelectric material with a tetragonal structure at room temperature.[30−33] The polarizations of the tetragonal BTO align along the ± [100], ± [010], and ± [001] axes, resulting in the coexistence of both 90° and 180° domains in the material.[5] Details of our sample preparation and experimental setup for in-situ compression experiments are provided in the Supporting Information. Figure 1a presents the in-situ domain switching behavior in a thin BTO micropillar with dimensions of ~3.0 μm × 1.7 μm × 0.07 μm (length × width × thickness). The polarization of a_1^+ domains is along the [100] axis and the polarization of a_2^- domains is aligned along the $[0\bar{1}0]$ axis. The initial a_1^+/a_2^- 90° domains with a head-to-tail polarization configuration were identified and are schematically shown in Figure 1a. The 90° domain configurations were determined by electron diffraction, which is presented in the Supporting Information. When a mechanical loading was applied to the micropillar, dense nanodomains formed within an a_2^- domain. The load−displacement curve indicates that the deformation of the micropillar is elastic (Supporting Information). The newly formed DWs between the nanodomains extend along the ± [100] direction. Figure 1b, c shows electron diffraction patterns recorded before and during the mechanical loading, respectively, which were obtained from the area marked with red circles in the TEM images in Figure 1a. There was no diffraction spot splitting before mechanical loading (Figure 1b), confirming the single-domain state of the a_2^- domain. When mechanical loading was applied to the micropillar, diffraction spot splitting occurred (Figure 1c), implying the evolution from a single domain to two types of domains. Diffraction spots split along the $[1\bar{1}0]^*$ direction, suggesting a relative 90°-rotation polarization relationship between the coexisting domains. Interestingly, these 90°-rotation-related domain complexes share the DWs along the [100] direction, resulting in a CDW feature with positive and negative bound charges at the lower and upper DWs of the a_2^- nanodomain, respectively, as shown in Figure 1d. The newly formed CDWs were stable when the mechanical loading was maintained at 12 μN. After removing the stress, all CDWs disappeared and the single a_2^- domain recovered (refer to the TEM image labeled 3 in Figure 1a). Note that CDWs formed only at places where the level of local compressive stress reached the threshold value for the CDW formation (Supporting Information) and that the initial domain structure would not fully recover if the applied stress were at a very high level (Supporting Information).

During the experiment, the ultrathin lamella may buckle or warp, leading to strain fluctuation in the material.[34] To evaluate the strain fluctuation in BTO lamellae caused by buckling, we carried out nonlinear buckling analysis in BTO lamellae with different thicknesses using FEA (Figure 2). Detailed information

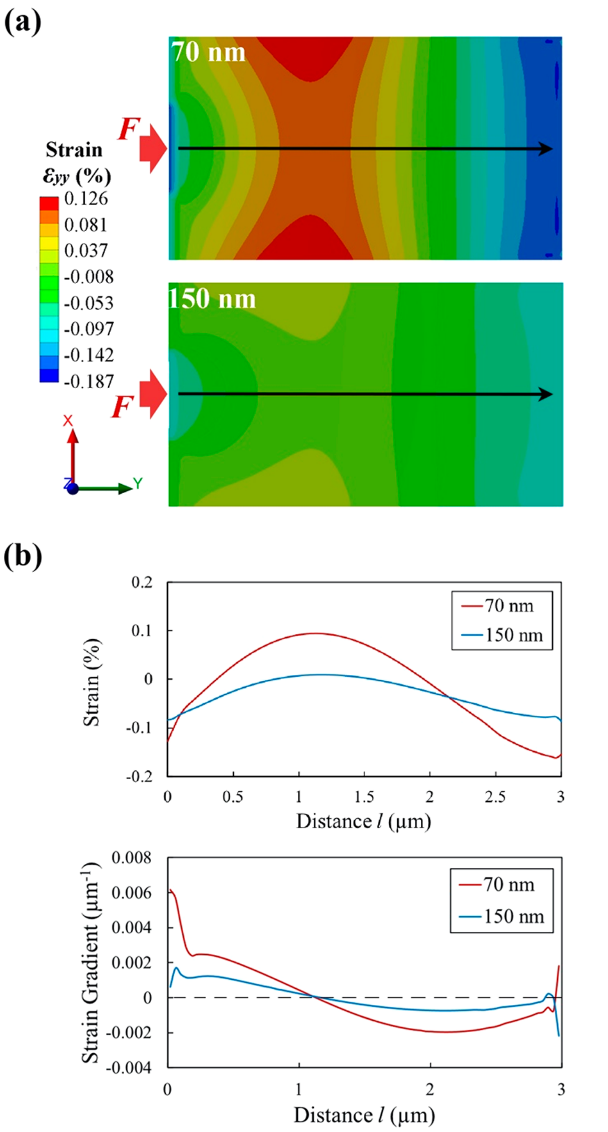

Figure 2. FEA of strain fluctuation in BTO lamellae with different thicknesses under compressive mechanical stress. (a) The strain (ε_{yy}) distribution of the BTO lamellae with thicknesses of 70 nm and 150 nm. (b) The strain (ε_{yy}) and strain gradient ($\frac{\partial \varepsilon_{yy}}{\partial l}$) along the black arrows of BTO lamellae in panel a.

on the FEA is presented in the Supporting Information. The strain (ε_{yy}) distributions in BTO lamellae with thicknesses of 70 nm and 150 nm at their experimentally applied loads of 12 μN and 27 μN, respectively, are presented in Figure 2a. As a result of the out-of-plane buckling, the strain state of the 70 nm thick lamella varied along the axial direction between tension and compression. The line profile analysis shown in Figure 2b was performed along the middle line parallel to the axial direction, as marked by the black arrows in Figure 2a. The corresponding strain gradient $\frac{\partial \varepsilon_{yy}}{\partial l}$, i.e., the derivative of the strain (ε_{yy}) with respect to the distance (l), is also shown in Figure 2b. Clearly, there exists a large strain gradient in the transition region between tensile and compressive strain. Specifically, the strain gradient peaks at ∼0.0025 μm^{-1} in the region where the strain state transforms from compression to tension whereas it reaches approximately −0.002 μm^{-1} in the region where tensile strain changes to compressive strain. The strain gradient fluctuates markedly at both ends of the model due to the constraint of their boundary conditions. The strain fluctuations give rise to high local strain gradients in ultrathin BTO lamellae. Internal structural changes must occur to accommodate these local strain gradients.[35] Indeed, a strong local lattice mismatch was observed in regions close to the head/tail-to-body 90° CDWs (Figure 1d), which is an energetically favorable way to accommodate the resultant local strain gradient in the thin lamellar system.

The significant role of the local strain gradient in the formation of this new type of 90° CDW is confirmed by bond-valence MD simulations[36,37] of an ultrathin BTO lamella subjected to compressive uniaxial strains (Figure 3). Detailed information on the MD simulations is presented in the Supporting Information. The compressive strain is increased from 0.5% to 2.0%, resembling the experimental setup in which the compressive loading changed from a low level to a high level. In the case of a low-level strain (0.5%), typical 90° DW motions are seen, which leads to a reduced volume fraction of the [010] domain unfavored by the compressive strain. In response to a medium level strain (1.0%), a new domain with polarization mostly aligned along the [100] direction emerges within the [010] domain. The polarization rotation is evident at the DWs separating different domains. When the strain increased to a high level (2.0%), nanodomains formed, which are separated by well-defined, sharp 90° CDWs extended along the [100] direction. Additional calculations were performed to extract the surface strain gradient of an ultrathin lamella in response to compressive loading (Supporting Information). It revealed that a large compressive strain of 2.0% can drive a significant change in the local strain profile, which is responsible for the formation of new domain structures with CDWs.

Our combined experimental and theoretical studies of the thin BTO lamella suggest that local strain gradients induced by the buckling or warping of the thin film material upon

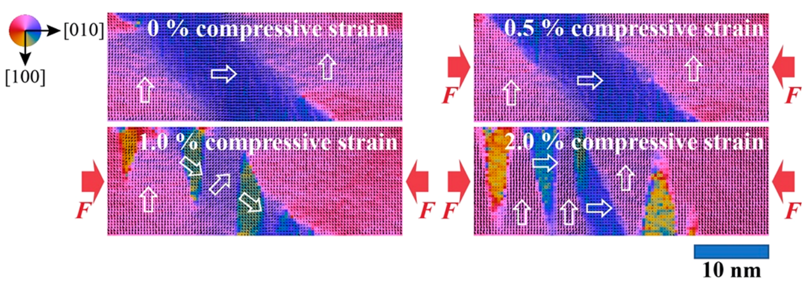

Figure 3. MD simulations of domain switching in an ultrathin BTO lamella under increased compressive mechanical stress. An increasing level of strain from 0.5% to 2.0% was applied to the lamella. The color wheel and the white arrows denote polarization directions.

compressive loading play a crucial role in the formation of the nanodomains separated by CDWs. Many studies have shown that the effect of the strain gradient is prominent mainly in materials with reduced dimensions.[35,38] Previous atomistic simulations revealed a strong scale-dependence of the strain gradient effect, i.e., piezoelectric and elastic properties could be greatly amplified with smaller size but weakened as the dimension increased.[39] These studies indicated that the effect of the strain gradient could be suppressed in thick samples. Therefore, experiments were carried out on thicker BTO lamellae but with the applied stress level unchanged to explore the response of domain structures to fewer strain gradients.

Here, the domain switching behavior of a thick BTO micropillar with dimensions of ~3.0 μm × 1.7 μm × 0.15 μm (length × width × thickness) was studied (Figure 4a). The initial

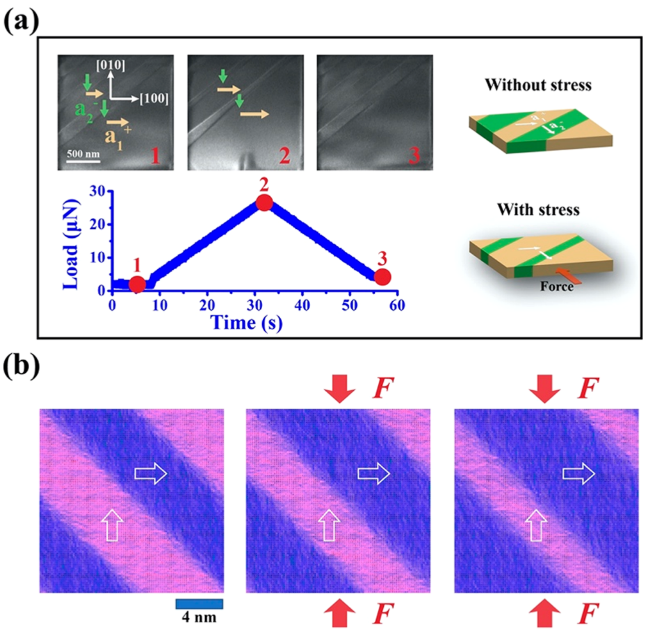

Figure 4. Domain switching behavior under a mechanical loading in a thick BTO. (a) In-situ TEM experiment of a thick BTO micropillar under a mechanical loading. Load versus time curve showing the real-time application of compressive load to the thick BTO micropillar. The numbers 1, 2, and 3 correspond to the TEM images (extracted from Movie S2) labeled 1, 2, and 3, respectively. Schematic diagrams of the domain configurations without and with the applied stress are presented at the right side. The yellow and green arrows in the TEM images and the white arrows in the schematics denote the polarization directions. (b) MD simulations of BTO under compressive mechanical stress with a bulk model. When a mechanical force is applied to the material from a low level to a high level, only the 90° DW motion occurs.

domains were also a_1^+/a_2^- 90° ferroelastic domains. Considering the difference in the cross-sectional area between this micropillar and the thin micropillar (Figure 1b), we precisely controlled the contact stress at a comparable level (~180 MPa in the thick sample and ~171 MPa in the thin sample) by controlling the maximum applied loads. In the thick micropillar, the applied stress drove the motion of the 90° ferroelastic DWs, resulting in the shrinkage of the a_2^- domains, and the expansion of the a_1^+ domains. This result is consistent with the observation of numerous previous studies that mechanical stress would induce DW motion in ferroelectrics composed of polydomains, rather than creating new DWs by forming nanodomains.[40−42] This consensus generally stands for thick ferroelectrics as the strain gradient was weakened in thick BTO lamellae under mechanical loading.

In addition, MD simulations of a bulk model (Figure 4b) were conducted, in which the buildup of the strain gradient was strictly forbidden due to the constraint of periodic boundary conditions along all directions. Contrary to the lamella model, the formation of nanodomains and CDWs was absent in the bulk system; instead, only conventional strain-driven 90° DW motion occurred, even at a high-level loading. This is also consistent with the lamella model simulations that only a large strain (gradient) could induce 90° CDWs, whereas a small strain (gradient) would only invoke 90° DW motions. The MD results suggest that the allowance of local strain gradients is essential for the formation of the head/tail-to-body 90° CDWs.

In previous studies, most of the bias- or thermal-induced CDWs are strongly CDWs.[10,28] A substantial amount of screening charges, which can compensate for the polarization charges, is required to stabilize the strong CDWs in ferroelectrics.[8] As ferroelectrics are mostly insulators with large band gaps, it is often difficult for free charge carriers to move in ferroelectrics,[43] hindering the mobility of CDWs. Our results show a new formation mechanism of CDWs that takes advantage of strain gradient without free charge carriers. In compliance with appropriate dimensions in BTO, the manipulation of substantial free carriers is not necessary, providing a controllable and reproducible strategy for the formation of CDWs. Flexoelectricity caused by giant strain gradients has been reported in BTO thin film of ~5 nm.[35] The prominent flexoelectric effect could induce 180° domain switching in BTO thin film. Our result is a successful complement to the study of strain gradient effect on ferroelectrics, from which CDWs could be produced with partial 90° domain switching. In addition to local strain gradients, the balance of different interfacial energies in the selected materials is also important for creating CDWs. A typical example is the formation of nanodomains in thin $Pb(Mg_{1/3}Nb_{2/3})$ O_3-38% $PbTiO_3$ (PMN-0.38PT), which is also a tetragonal ferroelectric material.[29] However, the newly formed domain walls between the nanodomains in PMN-0.38PT were along a ⟨110⟩ direction, indicating the formation of NDWs. Therefore, the observations that PMN-0.38PT and BTO lamellae adopt different nanodomain configurations indicate that the preference of the domain switching pathway in ferroelectrics is also determined by the concerted effects of various competing interfacial energies (Supporting Information).

CONCLUSIONS

In conclusion, a new type of 90° CDW with a head/tail-to-body configuration was produced in BTO by compression and was revealed by in-situ TEM. The formation of the 90° CDWs requires the presence of an appropriate strain gradient that can be provided by mechanical loading in a thin BTO. This study provides new insights into DWs in ferroelectrics and offers valuable guidance for the fabrication of nanoelectronics with reliable and reproducible CDWs.

ASSOCIATED CONTENT

Supporting Information

The Supporting Information is available free of charge at https://pubs.acs.org/doi/10.1021/acsami.2c14598.

https://doi.org/10.1021/acsami.2c14598
ACS Appl. Mater. Interfaces 2023, 15, 2313−2318

Details of sample preparation and experimental setup for in-situ compression experiments, common domain patterns and the corresponding electron diffraction patterns in BTO lamellae, load−displacement curve, effect of the level of local compressive stress, domain switching under high-level stress, finite element analysis, molecular dynamics simulations, evolution of surface strain in response to compressive loading and role of interfacial energies in the formation of CDWs (PDF)

Movie S1, domain switching behavior under mechanical loading in an ultra-thin BTO micropillar (MOV)

Movie S2, domain switching behavior under mechanical loading in a thick BTO micropillar (MOV)

AUTHOR INFORMATION

Corresponding Authors

Zibin Chen − *Department of Industrial and Systems Engineering, The Hong Kong Polytechnic University, Hong Kong, China*; Email: zi-bin.chen@polyu.edu.hk

Shi Liu − *Key Laboratory for Quantum Materials of Zhejiang Province, Department of Physics, School of Science, Westlake University, Hangzhou, Zhejiang 310030, China; Institute of Natural Sciences, Westlake Institute for Advanced Study, Hangzhou, Zhejiang 310024, China*; orcid.org/0000-0002-8488-4848; Email: liushi@westlake.edu.cn

Xiaozhou Liao − *School of Aerospace, Mechanical and Mechatronic Engineering, The University of Sydney, Sydney, New South Wales 2006, Australia*; orcid.org/0000-0001-8565-1758; Email: xiaozhou.liao@sydney.edu.au

Authors

Qianwei Huang − *School of Aerospace, Mechanical and Mechatronic Engineering, The University of Sydney, Sydney, New South Wales 2006, Australia*; orcid.org/0000-0003-1181-8089

Jiyuan Yang − *Key Laboratory for Quantum Materials of Zhejiang Province, Department of Physics, School of Science, Westlake University, Hangzhou, Zhejiang 310030, China; Institute of Natural Sciences, Westlake Institute for Advanced Study, Hangzhou, Zhejiang 310024, China*

Yujie Chen − *School of Mechanical Engineering, The University of Adelaide, Adelaide, South Australia 5005, Australia*; orcid.org/0000-0002-6588-6266

Matthew J. Cabral − *School of Aerospace, Mechanical and Mechatronic Engineering, The University of Sydney, Sydney, New South Wales 2006, Australia*

Haosu Luo − *Key Laboratory of Inorganic Functional Materials and Devices, Shanghai Institute of Ceramics, Chinese Academy of Sciences, Shanghai 200050, China*

Fei Li − *Electronic Materials Research Laboratory, Key Laboratory of the Ministry of Education, Xi'an Jiaotong University, Xi'an 710049, China*

Shujun Zhang − *Institute for Superconducting and Electronic Materials, Australian Institute of Innovative Materials, University of Wollongong, Wollongong, New South Wales 2522, Australia*; orcid.org/0000-0001-6139-6887

Yulan Li − *Pacific Northwest National Laboratory, Richland, Washington 99352, United States*; orcid.org/0000-0002-2431-5408

Zonghan Xie − *School of Mechanical Engineering, The University of Adelaide, Adelaide, South Australia 5005, Australia*

Houbing Huang − *School of Materials Science and Engineering, Beijing Institute of Technology, Beijing 100081, China*; orcid.org/0000-0002-8006-3495

Yiu-Wing Mai − *School of Aerospace, Mechanical and Mechatronic Engineering, The University of Sydney, Sydney, New South Wales 2006, Australia*

Simon P. Ringer − *School of Aerospace, Mechanical and Mechatronic Engineering, The University of Sydney, Sydney, New South Wales 2006, Australia*

Complete contact information is available at: https://pubs.acs.org/10.1021/acsami.2c14598

Author Contributions

Q.H., Z.C., and X.L. designed and directed the study. Q.H. and Z.C. conducted the in-situ TEM experiments and performed data analysis. J.Y. and S.L. performed MD simulations. Y.C. performed FEA. H.L. provided the samples. Q.H., Z.C., S.L., Y.C., and X.L. wrote the paper. All authors discussed the results and contributed to the paper.

Notes

The authors declare no competing financial interest.

ACKNOWLEDGMENTS

The authors acknowledge the facilities and the scientific and technical assistance of the Microscopy Australia node at the University of Sydney (Sydney Microscopy & Microanalysis). The authors acknowledge the financial support from the Australian Research Council Discovery Project DP190101155. J.Y. and S.L. acknowledge the supports from Westlake Foundation. The computational resource is provided by Westlake University Supercomputer Center. Z.C. acknowledges the financial support from the Research Office (Project code: P0039581 and P0042733) of The Hong Kong Polytechnic University.

REFERENCES

(1) Auciello, O.; Scott, J. F.; Ramesh, R. The Physics of Ferroelectric Memories. *Phys. Today* **1998**, *51* (7), 22−27.

(2) Cross, L. E. Ferroelectric Materials for Electromechanical Transducer Applications. *Mater. Chem. Phys.* **1996**, *43* (2), 108−115.

(3) Scott, J. Applications of Modern Ferroelectrics. *Science* **2007**, *315* (5814), 954−959.

(4) Chen, Z.; Li, F.; Huang, Q.; Liu, F.; Wang, F.; Ringer, S. P.; Luo, H.; Zhang, S.; Chen, L.-Q.; Liao, X. Giant Tuning of Ferroelectricity in Single Crystals by Thickness Engineering. *Sci. Adv.* **2020**, *6* (42), No. eabc7156.

(5) Merz, W. J. Domain Formation and Domain Wall Motions in Ferroelectric Bati O 3 Single Crystals. *Phys. Rev.* **1954**, *95* (3), 690.

(6) Jia, C.-L.; Mi, S.-B.; Urban, K.; Vrejoiu, I.; Alexe, M.; Hesse, D. Atomic-Scale Study of Electric Dipoles near Charged and Uncharged Domain Walls in Ferroelectric Films. *Nat. Mater.* **2008**, *7* (1), 57.

(7) Sluka, T.; Bednyakov, P.; Yudin, P.; Crassous, A.; Tagantsev, A.Charged Domain Walls in Ferroelectrics. In *Topological Structures in Ferroic Materials*; Springer, 2016; pp 103−138.

(8) Bednyakov, P. S.; Sturman, B. I.; Sluka, T.; Tagantsev, A. K.; Yudin, P. V. Physics and Applications of Charged Domain Walls. *npj Comput. Mater.* **2018**, *4* (1), 1−11.

(9) Sluka, T.; Tagantsev, A. K.; Damjanovic, D.; Gureev, M.; Setter, N. Enhanced Electromechanical Response of Ferroelectrics Due to Charged Domain Walls. *Nat. Commun.* **2012**, 3, 748.

(10) Catalan, G.; Seidel, J.; Ramesh, R.; Scott, J. F. Domain Wall Nanoelectronics. *Rev. Mod. Phys.* **2012**, *84* (1), 119.

(11) Wu, W.; Horibe, Y.; Lee, N.; Cheong, S. W.; Guest, J. R. Conduction of Topologically Protected Charged Ferroelectric Domain Walls. *Phys. Rev. Lett.* **2012**, *108* (7), 077203.

(12) Sharma, P.; Zhang, Q.; Sando, D.; Lei, C. H.; Liu, Y.; Li, J.; Nagarajan, V.; Seidel, J. Nonvolatile Ferroelectric Domain Wall Memory. *Sci. Adv.* **2017**, *3* (6), No. e1700512.
(13) Li, L.; Britson, J.; Jokisaari, J. R.; Zhang, Y.; Adamo, C.; Melville, A.; Schlom, D. G.; Chen, L. Q.; Pan, X. Giant Resistive Switching Via Control of Ferroelectric Charged Domain Walls. *Adv. Mater.* **2016**, *28* (31), 6574−6580.
(14) Jiang, J.; Bai, Z. L.; Chen, Z. H.; He, L.; Zhang, D. W.; Zhang, Q. H.; Shi, J. A.; Park, M. H.; Scott, J. F.; Hwang, C. S.; Jiang, A. Q. Temporary Formation of Highly Conducting Domain Walls for Non-Destructive Read-out of Ferroelectric Domain-Wall Resistance Switching Memories. *Nat. Mater.* **2018**, *17* (1), 49−56.
(15) Ma, J.; Ma, J.; Zhang, Q.; Peng, R.; Wang, J.; Liu, C.; Wang, M.; Li, N.; Chen, M.; Cheng, X.; Gao, P.; Gu, L.; Chen, L. Q.; Yu, P.; Zhang, J.; Nan, C. W. Controllable Conductive Readout in Self-Assembled, Topologically Confined Ferroelectric Domain Walls. *Nat. Nanotechnol.* **2018**, *13* (10), 947−952.
(16) Chai, X.; Jiang, J.; Zhang, Q.; Hou, X.; Meng, F.; Wang, J.; Gu, L.; Zhang, D. W.; Jiang, A. Q. Nonvolatile Ferroelectric Field-Effect Transistors. *Nat. Commun.* **2020**, *11* (1), 1−9.
(17) Småbråten, D. R.; Meier, Q. N.; Skjærvø, S. H.; Inzani, K.; Meier, D.; Selbach, S. M. Charged Domain Walls in Improper Ferroelectric Hexagonal Manganites and Gallates. *Phys. Rev. Mater.* **2018**, *2* (11), 114405.
(18) Jiang, A. Q.; Zhang, Y. Next-Generation Ferroelectric Domain-Wall Memories: Principle and Architecture. *NPG Asia Mater.* **2019**, *11* (1), 1−5.
(19) Guyonnet, J.*Ferroelectric Domain Walls: Statics, Dynamics, and Functionalities Revealed by Atomic Force Microscopy*; Springer Science & Business Media, 2014.
(20) Mantri, S.; Daniels, J. Domain Walls in Ferroelectrics. *J. Am. Ceram. Soc.* **2021**, *104* (4), 1619−1632.
(21) McQuaid, R. G.; Campbell, M. P.; Whatmore, R. W.; Kumar, A.; Gregg, J. M. Injection and Controlled Motion of Conducting Domain Walls in Improper Ferroelectric Cu-Cl Boracite. *Nat. Commun.* **2017**, *8* (1), 1−7.
(22) Bednyakov, P. S.; Sluka, T.; Tagantsev, A. K.; Damjanovic, D.; Setter, N. Formation of Charged Ferroelectric Domain Walls with Controlled Periodicity. *Sci. Rep.* **2015**, *5*, 15819.
(23) Ying, C. Y.; Muir, A. C.; Valdivia, C. E.; Steigerwald, H.; Sones, C. L.; Eason, R. W.; Soergel, E.; Mailis, S. Light-Mediated Ferroelectric Domain Engineering and Micro-Structuring of Lithium Niobate Crystals. *Laser Photonics Rev.* **2012**, *6* (4), 526−548.
(24) Guo, H.; Liu, X.; Rödel, J.; Tan, X. Nanofragmentation of Ferroelectric Domains During Polarization Fatigue. *Adv. Funct. Mater.* **2015**, *25* (2), 270−277.
(25) Huang, Q.; Chen, Z.; Cabral, M. J.; Wang, F.; Zhang, S.; Li, F.; Li, Y.; Ringer, S. P.; Luo, H.; Mai, Y.-W.; Liao, X. Direct Observation of Nanoscale Dynamics of Ferroelectric Degradation. *Nat. Commun.* **2021**, *12* (1), 2095.
(26) Chen, P.; Zhong, X.; Zorn, J. A.; Li, M.; Sun, Y.; Abid, A. Y.; Ren, C.; Li, Y.; Li, X.; Ma, X.; et al. Atomic Imaging of Mechanically Induced Topological Transition of Ferroelectric Vortices. *Nat. Commun.* **2020**, *11* (1), 1−8.
(27) Sato, Y.; Hirayama, T.; Ikuhara, Y. Real-Time Direct Observations of Polarization Reversal in a Piezoelectric Crystal: Pb (Mg 1/3 Nb 2/3) O 3- Pbtio 3 Studied Via in Situ Electrical Biasing Transmission Electron Microscopy. *Phys. Rev. Lett.* **2011**, *107* (18), 187601.
(28) Sluka, T.; Tagantsev, A. K.; Bednyakov, P.; Setter, N. Free-Electron Gas at Charged Domain Walls in Insulating Batio(3). *Nat. Commun.* **2013**, *4*, 1808.
(29) Chen, Z.; Hong, L.; Wang, F.; Ringer, S. P.; Chen, L.-Q.; Luo, H.; Liao, X. Facilitation of Ferroelectric Switching Via Mechanical Manipulation of Hierarchical Nanoscale Domain Structures. *Phys. Rev. Lett.* **2017**, *118* (1), 017601.
(30) Vijatović, M.; Bobić, J.; Stojanović, B. History and Challenges of Barium Titanate: Part I. *Science of Sintering* **2008**, *40* (2), 155.
(31) Sharma, P.; McQuaid, R. G.; McGilly, L. J.; Gregg, J. M.; Gruverman, A. Nanoscale Dynamics of Superdomain Boundaries in Single-Crystal Batio3 Lamellae. *Adv. Mater.* **2013**, *25* (9), 1323−1330.
(32) Wang, B.; Lu, H.; Bark, C. W.; Eom, C.-B.; Gruverman, A.; Chen, L.-Q. Mechanically Induced Ferroelectric Switching in Batio3 Thin Films. *Acta Mater.* **2020**, *193*, 151−162.
(33) Kim, D.; Jo, J.; Kim, Y.; Chang, Y.; Lee, J.; Yoon, J.-G.; Song, T.; Noh, T. Polarization Relaxation Induced by a Depolarization Field in Ultrathin Ferroelectric Batio 3 Capacitors. *Phys. Rev. Lett.* **2005**, *95* (23), 237602.
(34) Parrinello, M.; Rahman, A. Strain Fluctuations and Elastic Constants. *J. Chem. Phys.* **1982**, *76* (5), 2662−2666.
(35) Lu, H.; Bark, C.-W.; Esque de los Ojos, D.; Alcala, J.; Eom, C. B.; Catalan, G.; Gruverman, A. Mechanical Writing of Ferroelectric Polarization. *Science* **2012**, *336* (6077), 59−61.
(36) Liu, S.; Grinberg, I.; Takenaka, H.; Rappe, A. M. Reinterpretation of the Bond-Valence Model with Bond-Order Formalism: An Improved Bond-Valence-Based Interatomic Potential for Pbtio 3. *Phys. Rev. B* **2013**, *88* (10), 104102.
(37) Qi, Y.; Liu, S.; Grinberg, I.; Rappe, A. M. Atomistic Description for Temperature-Driven Phase Transitions in Batio 3. *Phys. Rev. B* **2016**, *94* (13), 134308.
(38) Nguyen, T. D.; Mao, S.; Yeh, Y. W.; Purohit, P. K.; McAlpine, M. C. Nanoscale Flexoelectricity. *Adv. Mater.* **2013**, *25* (7), 946−974.
(39) Majdoub, M.; Sharma, P.; Cagin, T. Enhanced Size-Dependent Piezoelectricity and Elasticity in Nanostructures Due to the Flexoelectric Effect. *Phys. Rev. B* **2008**, *77* (12), 125424.
(40) Gao, P.; Britson, J.; Nelson, C. T.; Jokisaari, J. R.; Duan, C.; Trassin, M.; Baek, S.-H.; Guo, H.; Li, L.; Wang, Y.; et al. Ferroelastic Domain Switching Dynamics under Electrical and Mechanical Excitations. *Nat. Commun.* **2014**, *5*, 3801.
(41) Alsubaie, A.; Sharma, P.; Lee, J. H.; Kim, J. Y.; Yang, C.-H.; Seidel, J. Uniaxial Strain-Controlled Ferroelastic Domain Evolution in Bifeo3. *ACS Appl. Mater. Interfaces* **2018**, *10* (14), 11768−11775.
(42) Lu, H.; Liu, S.; Ye, Z.; Yasui, S.; Funakubo, H.; Rappe, A. M.; Gruverman, A. Asymmetry in Mechanical Polarization Switching. *Appl. Phys. Lett.* **2017**, *110* (22), 222903.
(43) Li, L.; Gao, P.; Nelson, C. T.; Jokisaari, J. R.; Zhang, Y.; Kim, S.-J.; Melville, A.; Adamo, C.; Schlom, D. G.; Pan, X. Atomic Scale Structure Changes Induced by Charged Domain Walls in Ferroelectric Materials. *Nano Lett.* **2013**, *13* (11), 5218−5223.

https://doi.org/10.1021/acsami.2c14598
ACS Appl. Mater. Interfaces 2023, 15, 2313−2318